J. Mech. Phys. Solids 169 (2022) 105083

Contents lists available at ScienceDirect

Journal of the Mechanics and Physics of Solids

journal homepage: www.elsevier.com/locate/jmps

Fracture tolerance induced by dynamic bonds in hydrogels

Hang Yang [a,1], Xi Chen [b,1], Bonan Sun [b], Jingda Tang [b,*], Joost J. Vlassak [a,*]

[a] John A. Paulson School of Engineering and Applied Sciences, Harvard University, Cambridge, MA 02138, United States
[b] Department of Engineering Mechanics, State Key Laboratory for Strength and Vibration of Mechanical Structures, Xi'an Jiaotong University, Xi'an 710049, China

ARTICLE INFO

Keywords:
Hydrogel fatigue
Dynamic bonds
UV

ABSTRACT

Among soft materials, hydrogels with dynamic bonds that can be activated by a range of stimuli including temperature, pH, and infrared or ultraviolet light, constitute a special class of materials with unusual properties such as self-healing, actuation, and controlled degradation. Here, we take a hydrogel with reconfigurable disulfide crosslinks as an example and investigate its mechanical behavior. We demonstrate that this material has excellent fracture and fatigue resistance when the disulfide crosslinks are activated by ultraviolet illumination. We propose a simple constitutive model that describes the mechanical behavior of the material under a broad range of conditions.

1. Introduction

Hydrogels are a class of soft materials that consist of a hydrophilic polymer network dispersed in a matrix of water (Yang and Suo, 2018; Zhang and Khademhosseini, 2017). They are used in a broad range of applications because of their biocompatibility, stretchability, and similarity to biological tissue. Typical applications include drug delivery, wound dressing, artificial tissue, lubricating coatings, stretchable electronics, and soft machines (Li and Mooney, 2016; Liu et al., 2020; Yang and Suo, 2018; Yuk et al., 2019; Zhao et al., 2021). Hydrogels are also excellent model materials for fundamental research on polymers because they can be synthesized with relatively simple structures (Bai et al., 2019; Creton, 2017; Creton and Ciccotti, 2016; Kim et al., 2021; Wang et al., 2021; Yang et al., 2020).

While most hydrogels tend to be fragile, several hydrogels with extraordinary toughness in the range of 1000–10,000 J/m^2 have been developed. Examples include hydrogels with double networks (Gong et al., 2003; Sun et al., 2012), polyampholyte hydrogels (Sun et al., 2013), hydrogels crosslinked by metal ions (Lin et al., 2015), and nanoparticle reinforced hydrogels (Jiang et al., 2017). The key factor to improving the toughness of a hydrogel is to incorporate mechanisms that increase energy dissipation during fracture of the hydrogel. While these hydrogels have high toughness, recent research (Bai et al., 2019; Zhang et al., 2018a, 2018b) has demonstrated that their fatigue thresholds are determined mainly by the length of the polymer chains (Zhang et al., 2018b) and can be quite low (~50 J/m^2) (Bai et al., 2019; Zhang et al., 2018a, 2018b).

A number of strategies have been explored to improve the fatigue resistance of hydrogels. In a double-network hydrogel with a brittle short-chain network (poly(1-acrylamido-2-methylpropane sulfonic acid), PAMPS) and a long-chain network (polyacrylamide, PAAm), the long-chain network maintains the integrity of the hydrogel even after the brittle network fractures under load (Zhang et al., 2018b). The fatigue resistance depends on the length of the PAAm network and increases with the length of the polymer chains.

* Corresponding authors.
E-mail addresses: tangjd@mail.xjtu.edu.cn (J. Tang), vlassak@seas.harvard.edu (J.J. Vlassak).
[1] These authors contributed equally to this work.

https://doi.org/10.1016/j.jmps.2022.105083
Received 2 March 2022; Received in revised form 5 August 2022; Accepted 22 September 2022
Available online 1 October 2022

Fiber-reinforced composite structures (Wang et al., 2019; Yang et al., 2021) can also have a higher fatigue threshold as the fibers de-concentrate the stresses at the crack tip. This strategy has been applied to hydrogel-hydrogel, hydrogel-elastomer, and elastomer-elastomer systems (Wang et al., 2019; Xiang et al., 2020; Yang et al., 2021). Similarly, some hydrogels such as poly(vinyl alcohol)-based hydrogels contain stiff crystalline domains that can arrest crack growth, resulting in much-improved fatigue resistance (Lin et al., 2019a, 2019b).

While several mechanisms to enhance the fatigue resistance of hydrogels have been investigated, the use of controllable dynamic crosslinks for this purpose has not been explored extensively thus far. Hydrogels that consist of polymer networks with dynamic bonds can exhibit unusual properties such as the ability to self-heal or respond to environmental stimuli, and they may be easier to recycle (Guo et al., 2016; Long et al., 2014; Ma et al., 2014; Venkata et al., 2021; Zheng et al., 2021). The constitutive behavior of hydrogels with dynamic reactions or self-healing ability (Guo et al., 2016; Long et al., 2014; Venkata et al., 2021) has been investigated previously, but there are only few reports on the effects of dynamic crosslinks on the fracture and fatigue behavior of hydrogels (Guo et al., 2018; Li et al., 2021; Li and Gong, 2022; Xiao et al., 2022).

Here, we investigate a hydrogel with reconfigurable dynamic bonds (Fig. 1a). We take a PAAm hydrogel that is crosslinked with disulfide bonds as an example (Fig. 1b). The disulfide bonds break and reform when they interact with radicals that are generated in the hydrogel by UV illumination (Chen et al., 2019; Du et al., 2015; Fairbanks et al., 2011). This dynamic process of breaking and reforming crosslinks (Fig. 1c) has a profound effect on the mechanical behavior of the hydrogel which is well described by a viscoplastic model that connects the plastic flow of the hydrogel under UV illumination with the radical concentration in the hydrogel. Our results show that the viscoplastic flow that results from this dynamic process of crosslink reconfiguration is effective at reducing crack growth under both static and dynamic loading conditions and improves the critical fracture stretch, fracture toughness, and even the fatigue threshold of the hydrogel.

2. Materials and methods

Materials All the chemicals are used as purchased without further purification. Acrylamide (AAm), ammonium persulfate (APS), N, N-Methylenebisacrylamide (MBAA), and 2-hydroxy-4′-(2-hydroxyethoxy)-2-methylpropiophenone (I2959) were purchased from

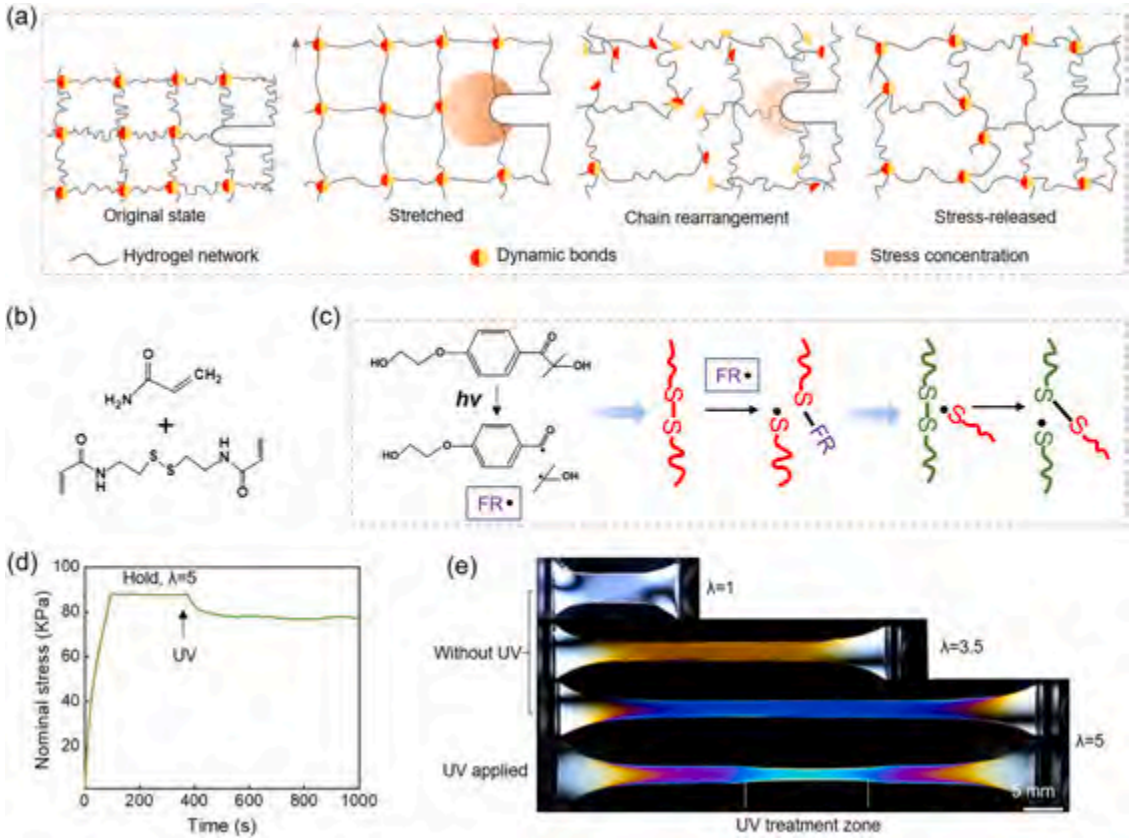

Fig. 1. Dynamic bonds and stress relief. (a) Illustration of the dynamic bonds reconfiguration and stress release. (b) The hydrogel is synthesized using AAm as monomer and BAC as crosslinker. (c) Free radicals formed as a result of UV illumination attack the disulfide bonds, breaking and reforming crosslinks. (d) The stress-time curve shows stress relaxation under UV illumination. (e) Birefringence images of stretched specimens using polarized light showing stress contours.

Aladdin®. N, N, N', N'-tetramethylethylenediamine (TEMED), N, N'- bis (acryloyl) cystamine (BAC), and methanol were purchased from Sigma-Aldrich.

Hydrogel fabrication The hydrogel was synthesized using 28.4 wt% Acrylamide (AAm), 0.02–0.1 wt% BAC, methanol (five times the weight of BAC), 0.1–0.5 wt % photoinitiator I2959, in deionized water. All materials were mixed to obtain a uniform solution by magnetic stirring. Then, 0.0684 wt% APS and 0.6 μL/g TEMED relative to the solution were added as heat initiators. For MBAA crosslinked hydrogel, the BAC is replaced with 0.03 wt% MBAA. The solution was cast into a mold consisting of two glass plates and a silicone spacer with a thickness of 1 mm and was stored at room temperature for six hours until full gelation.

Hydrogel adhesion and peeling Hydrogel samples (with 0.05 wt% BAC and 0.5 wt% PI, 1 mm in thickness) were cut into 20 x 50 mm rectangles. Two such pieces of hydrogel were stacked on top of each other and exposed to UV (2 mW/cm^2) for different lengths of time. A strip of paper was glued to the back of the hydrogel strips to constrain deformation during the test. The peel test was performed on a mechanical test machine (AGS-X) with a 100 N load cell at a crosshead speed of 50 mm/min. The displacement and force curves were recorded, and the adhesion energy was calculated as $2F/w$, where F is the steady-state peeling force and w is the width of the samples.

Oscillation, creep, relaxation The oscillation and creep tests for the hydrogel were performed by DMA Q800 (TA Instruments). The hydrogel samples were fabricated into a strip with a gauge length of 8 mm and a width of 4 mm using a cutter. The storage and loss moduli of the hydrogel were measured as a function of frequency at a strain of 0.1 without UV illumination. To evaluate the effect of UV on the storage and loss moduli, an oscillation experiment was performed at a frequency of 1 Hz. For the creep tests, specimens were held at different nominal stress levels and the corresponding stretch was recorded with a sampling interval of 0.5 s/point. For creep experiments under UV illumination, the load was applied to the sample one minute before the UV was turned on. Then UV with an intensity of 80 mW/cm^2 was applied for a duration of 300 s. For the relaxation experiments under UV illumination, a fixed displacement was applied to the sample one minute before the UV was turned on. Then UV with an intensity of 80 mW/cm^2 was applied for the duration of the experiment.

Tensile testing Pure-shear specimens were fabricated in a rectangular shape, with a length of 50 mm, and a width of 30 mm using a cutter. Acrylic plates were glued to the pure-shear samples leaving an actual gauge length of 10 mm. Tensile tests were performed using a universal mechanical test machine (AGS-X) with a 100 N load cell. UV light was applied using an OmniCure^{TM} Series 2000 with an average intensity of 80 mW/cm^2 (measured by radiometer photometer ILT1400). The light polarization system consisted of two polarizers, one in front of and one behind the specimen. All images and videos were recorded using a Canon EOS 5D camera.

Hydrogel toughness We used the pure-shear test to measure the toughness of the hydrogels. Specimens were cut into 30 x 50 mm rectangles using a cutter. Acrylic plates were glued to the samples leaving an actual gauge length of 10 mm only. Samples with pre-cracks had a pre-crack of 20 mm made by cutting the sample using a razor blade. Samples with and without pre-cracks were deformed at a constant crosshead speed. For UV-treated specimens, UV light (80 mW/cm^2) was applied for the duration of the test. For specimens with prior UV treatment, UV was applied to the specimens for 3 min, which were then stored for 2–3 min before testing.

Delayed fracture Pure-shear specimens were fabricated using the same procedure as for the toughness measurements, with a BAC concentration of 0.1 wt% and PI 0.5 wt%. Specimens with pre-cracks were deformed at a rate of 0.08 s^{-1} to a predefined stretch and the crack length was then recorded using a camera Canon EOS 5D. The energy release rate was calculated from the corresponding stretch-stress curve for specimens without pre-crack. In experiments with UV illumination, the UV light was turned on at the same time as the deformation of the sample was initiated.

Fatigue test Fatigue tests were performed on pure-shear specimens using a universal mechanical test machine (AGS-X). Specimens with pre-cracks were cycled to several stretches and the crack length was recorded by the camera. Specimens without pre-cracks were cycled to the same stretches, and the displacement-stress curves were recorded. The crosshead speed during the fatigue test was 10 mm/s, while individual stress-stretch curves were measured at 50 mm/min at specific times during the fatigue test. An environmental chamber was used to avoid dehydration. For the UV-treated specimens, UV (80 mW/cm^2) was applied for a duration of two minutes at the start of the test to activate the dynamic reaction, followed by continuous illumination of 2 mW/cm^2 during the remainder of the fatigue test. For specimens with prior UV treatment, UV was applied to the specimens for a duration of three minutes, after which they were stored for two to three minutes before fatigue testing.

3. Results and discussion

3.1. Dynamic reaction in the hydrogel

Fig. 1a illustrates the concept of stress relief as a result of hydrogel cross-link reconfiguration. When a hydrogel is stretched from its equilibrium state, the polymer network is under tension. As the dynamic crosslink system is activated by an external stimulus – in this case, the radicals generated by UV illumination – reconfiguration of the crosslinks occurs: chains under tension break at the dynamic bonds and rearrange to connect to other chains, reducing overall tension in the network. This process reduces the stress inside the bulk of the hydrogel and is expected to have a significant effect on the elevated stresses in the vicinity of a crack tip.

We demonstrate this idea using a hydrogel with a simple structure that consists of a polyacrylamide network crosslinked with disulfide bonds. The hydrogel is synthesized using acrylamide (AAm) as monomer and N, N'- bis (acryloyl) cystamine (BAC) as a dynamic crosslinker (Fig. 1b). In addition to the thermal initiators for the polymerization of acrylamide, a photoinitiator (PI, I2959) was used to produce free radicals on exposure to UV (Du et al., 2015; Fairbanks et al., 2009, 2011). These free radicals react with the disulfide bonds in the hydrogel to form thiyl radicals, which, in turn, react with other disulfide bonds to reconfigure the polyacrylamide network (Fig. 1c) thus reducing the stress in the network (Chen et al., 2019; Du et al., 2015; Fairbanks et al., 2011; Long et al., 2009).

The effect of UV illumination is illustrated in Fig. 1d, e. When a tensile specimen of this hydrogel is held at a stretch of $\lambda = 5$, the tensile stress in the specimen does not change with time. Illumination with UV, however, results in an almost instantaneous decrease in the stress level in the specimen (Fig. 1d). The birefringence images of stretched specimens in Fig. 1e were obtained using polarized light and show different colors depending on the stress level. The change in color upon UV illumination is obvious.

While the above results demonstrate that disulfide crosslinks break when the hydrogel is exposed to UV, they do not necessarily imply that new crosslinks form, even though crosslink rearrangement has been reported under different conditions (Chen et al., 2019; Du et al., 2015; Fairbanks et al., 2011). We now demonstrate using adhesion testing that crosslinks indeed recover after disruption. Hydrogel specimens are fabricated into strips and laid on top of each other without applying any pressure. Specimens in the test groups are UV treated for different periods to activate the dynamic bonds, while specimens in the control group (without UV treatment) are kept in the dark. The adhesion between the pieces of hydrogel is then measured using the peel test. Peel test results show that the adhesion energy reaches 18.0 ± 4.6 J/m^2 after five minutes of UV exposure and 81.2 ± 11.6 J/m^2 after two hours of exposure. By contrast, specimens in the control group that were not subjected to UV had adhesion energy of only 4.1 ± 0.6 J/m^2. These adhesion measurements demonstrate that new disulfide bonds form after disruption of network crosslinks by free radicals (An et al., 2022) (Fig. 2a–c).

Oscillatory DMA experiments were performed to measure the storage and loss moduli of the hydrogel both without and with UV illumination (Fig. 2d–f). The storage modulus is much larger than the loss modulus at the measurement frequency indicating that the hydrogel behaves mostly elastically. The change in the storage modulus of the hydrogel upon exposure to UV is within the experimental uncertainty of the measurement. There is, however, a small increase in the loss modulus upon UV exposure.

3.2. Model description

Here we describe a constitutive model that connects the UV illumination to the mechanical response of the hydrogel. The model is based on a model proposed by Ma et al (Long et al., 2009; Ma et al., 2014). These authors use a photo-viscoplastic model that depends on the radicals produced in a photochemical reaction to describe the relaxation and creep of a light-active polymer. In this model, the viscoplastic strain rate tensor is taken directly proportional to the deviatoric part of the total stress tensor with a proportionality constant that depends on the concentration of radicals. We use a similar model to describe the constitutive behavior of the hydrogel under UV illumination, but neglect any viscoelastic contribution to the deformation given the negligible viscoelastic strain when the hydrogel is deformed in the absence of UV. We characterize the viscoplastic flow rule by performing a series of creep experiments under UV illumination and show that the viscoplastic strain rate changes linearly with applied stress. The resulting model accurately

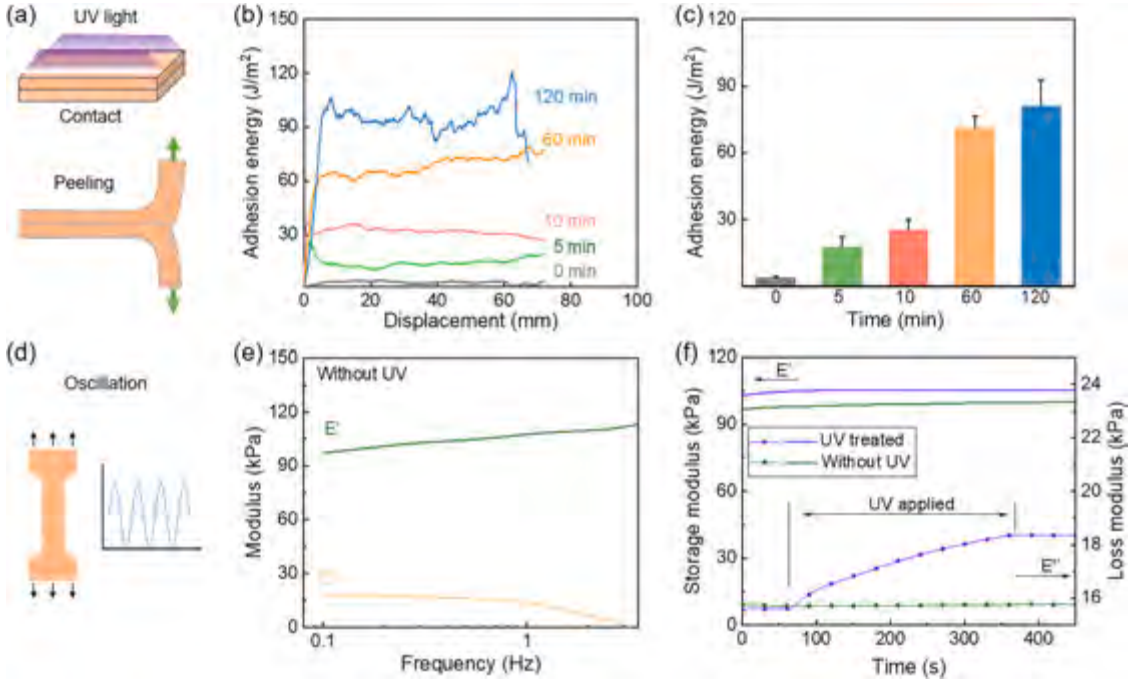

Fig. 2. Disruption and formation of new crosslinks within the hydrogel upon UV illumination. (a) Two pieces of the hydrogel are placed on top of each other and UV light with an intensity of 2 mW/cm^2 is applied for reaction activation. A peel test is performed to measure the adhesion between the hydrogel strips. (b) Peeling curves after various treatment periods and (c) the corresponding adhesion energies. (d) Schematic illustration of the DMA oscillation test performed on a hydrogel sample. (e) Evolution of the storage (E′) and loss (E″) moduli as a function of frequency in the absence of UV. (f) Evolution of the storage (E′) and loss (E″) moduli with time under UV irradiation. The applied nominal strain is 10% and measurements are performed at a frequency of 1 Hz. The concentration of BAC in the samples is 0.05 wt%, and PI is 0.5 wt%.

captures the behavior of the gel under a range of loading conditions both in the presence and the absence of UV illumination.

3.2.1. Photochemical reaction

Consider a hydrogel that consists of a polymer network linked together with bonds that are susceptible to disruption by free radicals produced by a photoinitiator upon UV illumination. We model the photoinitiation process as a first-order photochemical reaction, where we ignore any spatial non-uniformity of UV intensity or any attendant transport of reactants by diffusion. The concentration of the photoinitiator then evolves with time as described by (Long et al., 2009; Ma et al., 2014)

$$\frac{\partial C_I(t)}{\partial t} = -\beta I C_I(t), \tag{1}$$

where $C_I(t)$ is the photoinitiator concentration in the hydrogel, β is the photoinitiator molar absorption constant in units of $m^2s^{-1}W^{-1}$, and I is the intensity of the UV light in units of Wm^{-2}. If each photoinitiator produces m radicals upon absorption of a UV photon and $m = 2$ for our reaction (Fairbanks et al., 2009), the concentration of radicals evolves as

$$\frac{\partial C_R}{\partial t} = m\beta I C_I - k_o[C_R(t)]^\delta. \tag{2}$$

The second term on the right-hand side of this equation represents the decrease in radical concentration as a result of termination reactions, which result in the inactivation of the radical species. Termination occurs when two radicals encounter each other and recombine (Long et al., 2009). The symbol k_o represents the corresponding effective rate constant, and δ the reaction order, which corresponds to the number of radicals needed for a termination event. Assuming that radicals are terminated by reacting with another radical, we take $\delta = 2$. Eq. (2) contains two unknown parameters k_o and β, which will be determined later. Note that we have lumped together in Eq. (2) both the free radicals produced by the photoinitiator and the thiyl radicals generated by the reaction of the free radicals with the disulfide crosslinks.

3.2.2. Constitutive model

Elastic deformation in the absence of UV illumination. Fig. 3a shows a typical stress-stretch curve for a uniaxial tensile experiment performed without UV illumination. Fig. 3b shows a typical stress-stretch curve for a pure-shear experiment, also performed without UV illumination. In the absence of UV exposure, we describe the stress-stretch behavior of the hydrogel using a one-term Ogden model. The energy density for the Ogden model is given by Ogden (1972)

$$W = \frac{2\mu}{\alpha^2}\left(\lambda_{e1}^{\alpha} + \lambda_{e2}^{\alpha} + \lambda_{e3}^{\alpha} - 3\right). \tag{3}$$

In this expression, μ is the shear modulus, α is a material constant, λ_e is the elastic stretch, and the numerical subscripts refer to the principal directions. Assuming incompressibility, the Cauchy stress-stretch relation for elastic uniaxial tension is then given by

$$\sigma^U = H(\lambda_e) = \frac{2\mu}{\alpha}\left(\lambda_e^{\alpha} - \lambda_e^{-\alpha/2}\right), \tag{4a}$$

and the nominal stress is

$$S^U = \frac{\sigma^U}{\lambda_e} = \frac{2\mu}{\alpha}\left(\lambda_e^{\alpha-1} - \lambda_e^{-\alpha/2-1}\right). \tag{4b}$$

The Cauchy stress-stretch relation for a pure-shear specimen is given by

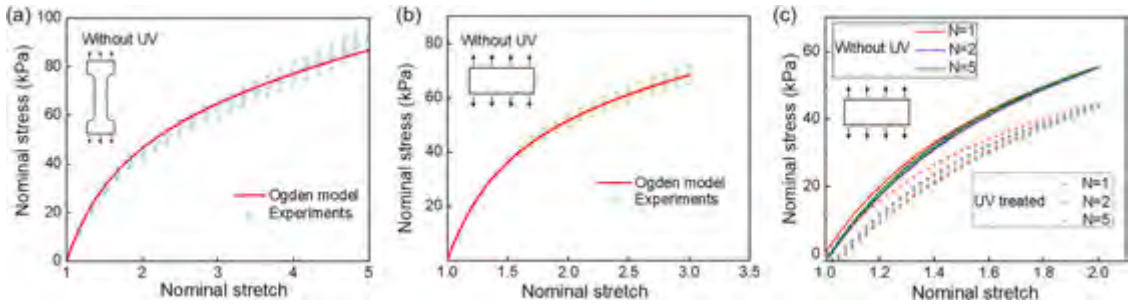

Fig. 3. Tensile experiments. (a) Experimental stress-stretch curve for a uniaxial tensile specimen along with the Ogden model fit to the data (no UV illumination), and (b) experimental stress-stretch curve for a pure-shear specimen along with the Ogden model fit (no UV illumination). (c) Stress-stretch curves consist of N load cycles with/without UV treatment. The concentration of BAC in the samples is 0.05 wt%, and PI is 0.5 wt%.

$$\sigma^{PS} = \frac{2\mu}{\alpha}\left(\lambda_e^{\alpha} - \lambda_e^{-\alpha}\right), \tag{5a}$$

while the corresponding nominal stress-stretch relation is

$$S^{PS} = \frac{\sigma^{PS}}{\lambda_e} = \frac{2\mu}{\alpha}\left(\lambda_e^{\alpha-1} - \lambda_e^{-\alpha-1}\right). \tag{5b}$$

It is evident from the figures that the Ogden model provides good fits to the experimental data both for the uniaxial (Fig. 3a) and the pure-shear specimens (Fig. 3b) in the absence of UV illumination. Note that the hydrogel shows very little hysteresis when not exposed to UV (Fig. 3c). Fitting Eqs. (4b) and (5b) to the experimental data yields values of 31.7 ± 1.5 kPa and 1.44 ± 0.06 for μ and α, respectively.

Viscoplastic flow under UV illumination. On exposure to UV, the photoinitiator produces free radicals that react with the disulfide crosslinks in the hydrogel to create dangling polymer chains terminated in thiyl radicals. Even though the concentration of radicals is comparable to the concentration of crosslinks in the hydrogel, the stiffness of the hydrogel remains largely unchanged under UV illumination (Fig. 2f). This experimental observation suggests that the free radicals do not fully disrupt the polyacrylamide network, but instead initiate a continuous process of severing and reforming the crosslinks (Fig. 1c): Free radicals react with crosslinks to form dangling polymer chains that are terminated in thiyl radicals. These thiyl radicals, in turn, react with other crosslinks to break and form new crosslinks, thus allowing the network to deform plastically in the presence of applied stress. Since the plastic flow of the hydrogel is mediated by the presence of radicals, we take the plastic strain rate proportional to the concentration of radicals in the hydrogel (Ma et al., 2014), but we do not specify the dependence on the applied stress $f(\sigma)$. The plastic strain rate for a uniaxial tension experiment then takes the form

$$\dot{\varepsilon}_p = \zeta C_R(t) f(\sigma), \tag{6}$$

where $\zeta$is a material constant and the functional form of $f(\sigma)$ is determined from a series of uniaxial creep experiments. The creep experiments were performed by applying constant forces to uniaxial tensile specimens and measuring the total stretches λ_t of the samples as a function of time. Without UV irradiation, the length of the specimens does not change with time after the load is applied (Fig. S1). Fig. 4a shows the results for samples subjected to various loads under UV irradiation. Because the deformation in the creep experiments is not small, the Cauchy stress and hence the elastic deformation of the samples varies throughout the experiment even though the applied force is constant. The Cauchy stress is calculated from the nominal stress S as $\sigma = S\lambda_t$ and is shown in Fig. 4b. Once the Cauchy stress is known, the elastic (Fig. 4c) and plastic (Fig. 4d) stretches are readily determined using Eq. (4a). Fig. 4e finally shows the evolution of the plastic strain rate $\dot{\varepsilon}_p$ during the experiment. To determine the functional dependence of the plastic strain rate on the applied stress, it is convenient to first eliminate the dependence on the radical concentration by normalizing all the plastic strain rate curves in Fig. 4e by the plastic strain rate curve obtained at a given applied nominal stress. In this case, the data in Fig. 4e was normalized by the average plastic strain rate curve, denoted as $\dot{\widetilde{\varepsilon}}_p$, obtained for an applied nominal stress of 60 kPa and a corresponding Cauchy stress $\widetilde{\sigma}$ (Fig. 4g). The result is shown in Fig. 4f. It is evident that this procedure has made the strain rate nearly independent of time. The normalized strain rate curves have the form

$$\dot{\varepsilon}_p / \dot{\widetilde{\varepsilon}}_p = f(\sigma)/f(\widetilde{\sigma}). \tag{7}$$

If $\dot{\varepsilon}_p$ has a power law dependence on σ, then a graph of $\dot{\varepsilon}_p/\dot{\widetilde{\varepsilon}}_p$ versus $\sigma/\widetilde{\sigma}$ should allow easy determination of the exponent. The results are shown in Fig. 4h and i. Evidently, the relationship between $\dot{\varepsilon}_p/\dot{\widetilde{\varepsilon}}_p$ and $\sigma/\widetilde{\sigma}$ is linear, so that

$$\dot{\varepsilon}_p = \zeta C_R(t)\sigma. \tag{8}$$

This expression is similar to that derived by Ma et al. (2014) (Long et al., 2009) based on a polymer physics model.

Once the functional dependence on the stress is known, the evolution of the radical concentration can be determined as a function of time since $C_R \sim \dot{\varepsilon}_p/\sigma$. Fig. 5 shows the evolution of this quantity for the various creep experiments. All curves collapse very nearly into a single master curve that scales with the evolution of the radicals in the hydrogel (Fig. 5a). A fit of the photochemistry model to this master curve then provides values for the remaining model parameters: $\beta = 1.17 \pm 0.02 \times 10^{-5}$ $\mathrm{m^2 s^{-1} W^{-1}}$, $k_o = 2.8 \pm 0.21 \times 10^{-3}$ $\mathrm{m^3 s^{-1} mol^{-1}}$, and $\zeta = 9.6 \pm 0.31 \times 10^{-7} \mathrm{m^3 s^{-1} kPa^{-1}}$. Fig. 5b shows the evolution of the photoinitiator and radical concentrations at a UV intensity of 80 $\mathrm{mW/cm^2}$ calculated using these model parameters. The same set of parameters leads to a much lower radical concentration and a much more gradual evolution of the concentrations at lower UV intensity (Fig. S2).

Kinematics of finite deformation. When exposed to UV, the hydrogel deforms both elastically and viscoplastically. We describe the kinematics of this deformation by assuming the existence of an intermediate, elastically unloaded configuration. The total deformation gradient tensor $\boldsymbol{F}_t$ then consists of two contributions, a viscoplastic contribution followed by an elastic contribution:

$$\boldsymbol{F}_t = \boldsymbol{F}_e \boldsymbol{F}_{vp} \tag{9}$$

where $\boldsymbol{F}_e$ is the deformation gradient tensor corresponding to the elastic deformation and $\boldsymbol{F}_{vp}$ is the deformation gradient tensor

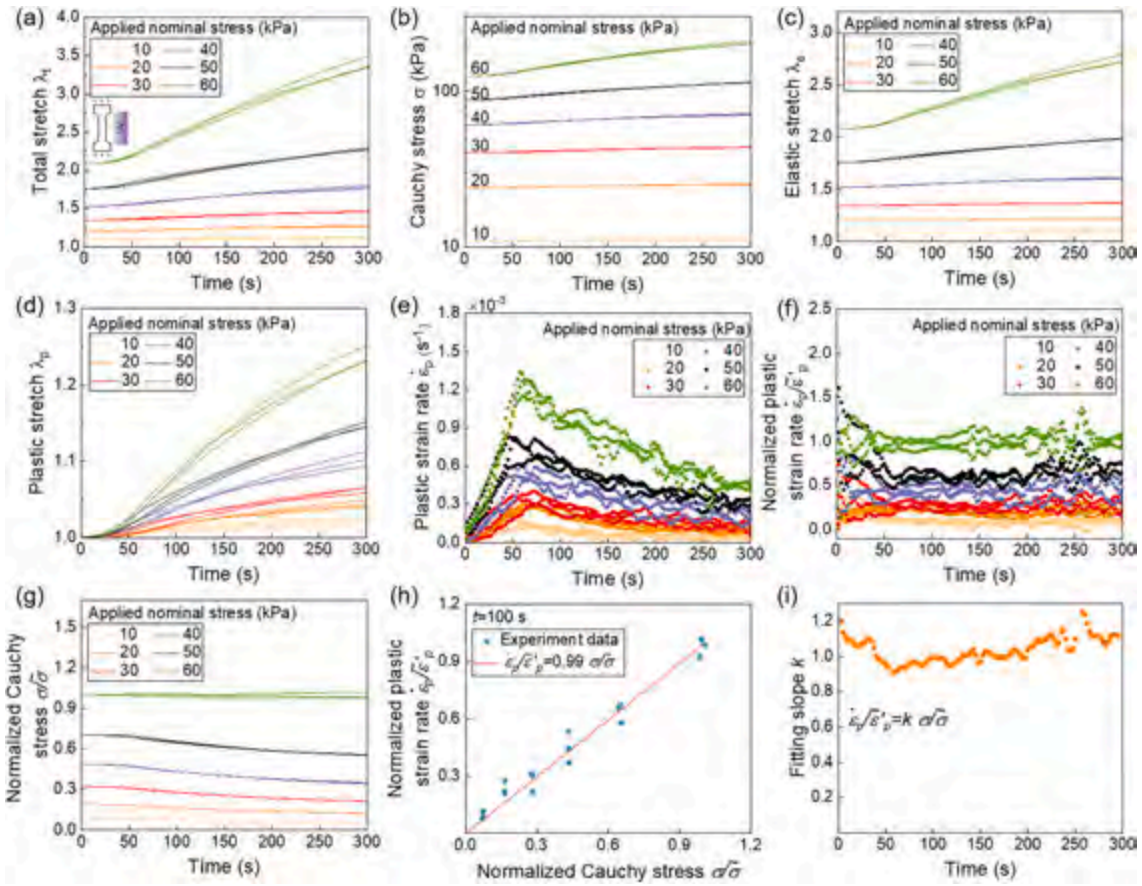

Fig. 4. Uniaxial creep experiments for various values of applied nominal stress performed under UV illumination. (a–d) The total stretch, Cauchy stress, elastic stretch, and viscoplastic stretch during the creep experiments. (e) Logarithmic plastic strain rates. (f, g) Normalized logarithmic plastic strain rates and normalized Cauchy stress. (h) The scatter plot and linear fitting for the normalized Cauchy stress and normalized logarithmic plastic strain rates at $t = 100$ s, and (i) the slopes of the linear fit at a given time for the entire duration of the UV irradiation. The concentration of BAC in the samples is 0.05 wt%, and PI is 0.5 wt%.

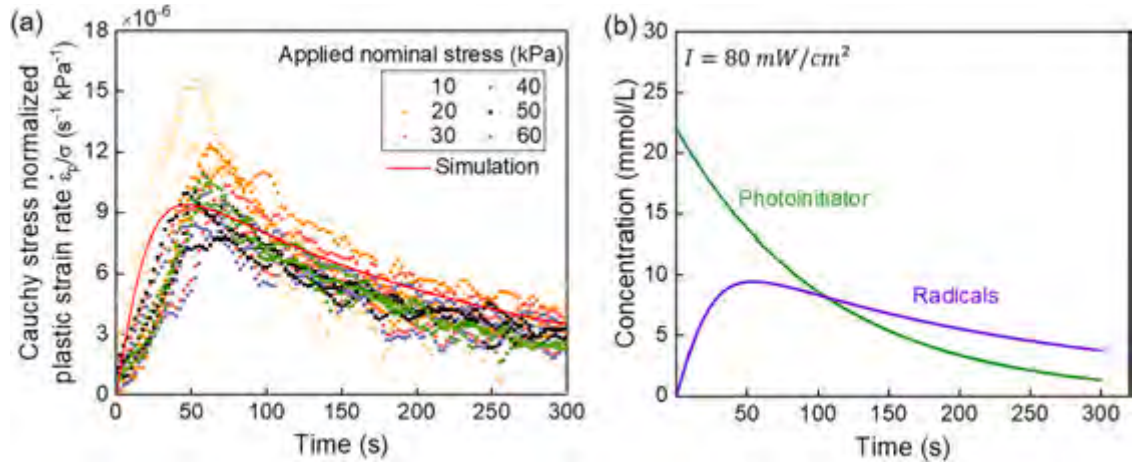

Fig. 5. (a) Cauchy stress normalized plastic strain rate under different nominal stress and the simulation curve. (b) The evolution of the photo-initiator and radical concentrations obtained from the photochemical model. The concentration of BAC in the samples is 0.05 wt%, and PI is 0.5 wt%.

corresponding to the viscoplastic deformation. The spatial velocity gradient $\boldsymbol{L}_t$ associate with the deformation is then defined as

$$\boldsymbol{L}_t = \dot{\boldsymbol{F}}_t \boldsymbol{F}_t^{-1} = \dot{\boldsymbol{F}}_e \boldsymbol{F}_e^{-1} + \boldsymbol{F}_e \dot{\boldsymbol{F}}_{vp} \boldsymbol{F}_{vp}^{-1} \boldsymbol{F}_e^{-1} = \boldsymbol{L}_e + \boldsymbol{F}_e \boldsymbol{L}_p \boldsymbol{F}_e^{-1}, \tag{10}$$

where $\boldsymbol{L}_e$ and $\boldsymbol{L}_p$ are the velocity gradients associated with the elastic and viscoplastic deformation fields, respectively. The viscoplastic velocity gradient $\boldsymbol{L}_p$ can be written as the sum of a symmetric and an antisymmetric part, thus defining the viscoplastic stretch tensor $\boldsymbol{D}_{vp}$ and the viscoplastic spin tensor $\boldsymbol{\Omega}_{vp}$, respectively,

$$\boldsymbol{L}_p = \boldsymbol{D}_{vp} + \boldsymbol{\Omega}_{vp}. \tag{11}$$

Following an argument by Weber and Anand (Weber and Anand, 1990), we attribute all rotations to the elastic component of the deformation, which leads to $\boldsymbol{\Omega}_{vp} = 0$ and $\boldsymbol{D}_{vp} = \boldsymbol{L}_p$. We then use Eq. (6) to define the flow rule for the viscoplastic deformation,

$$\boldsymbol{D}_{vp} = \frac{3}{2}\dot{\varepsilon}_p \frac{\boldsymbol{T}}{\sigma_{eq}} = \frac{3}{2}\zeta C_R(t) f(\sigma_{eq}) \frac{\boldsymbol{T}}{\sigma_{eq}}, \tag{12}$$

where $\boldsymbol{T}$ is the deviatoric component of the Cauchy stress tensor, $\sigma_{eq} = \sqrt{\frac{3}{2} T_{ij} T_{ij}}$ is the equivalent stress, and we have taken $\sigma = \sigma_{eq}$ in Eq. (6). Eq. (12) assumes that the viscoplastic flow is deviatoric, i.e., there is no volume change associated with the deformation process. While it is certainly possible that there is a small volume change associated with the creation of radicals upon UV illumination, the deformation process, which consists of a continuous breaking and reforming of bonds, should not result in a net change in the volume of the hydrogel. Taking a linear dependence of the viscoplastic strain rate on the stress as Eq. (8), we finally find

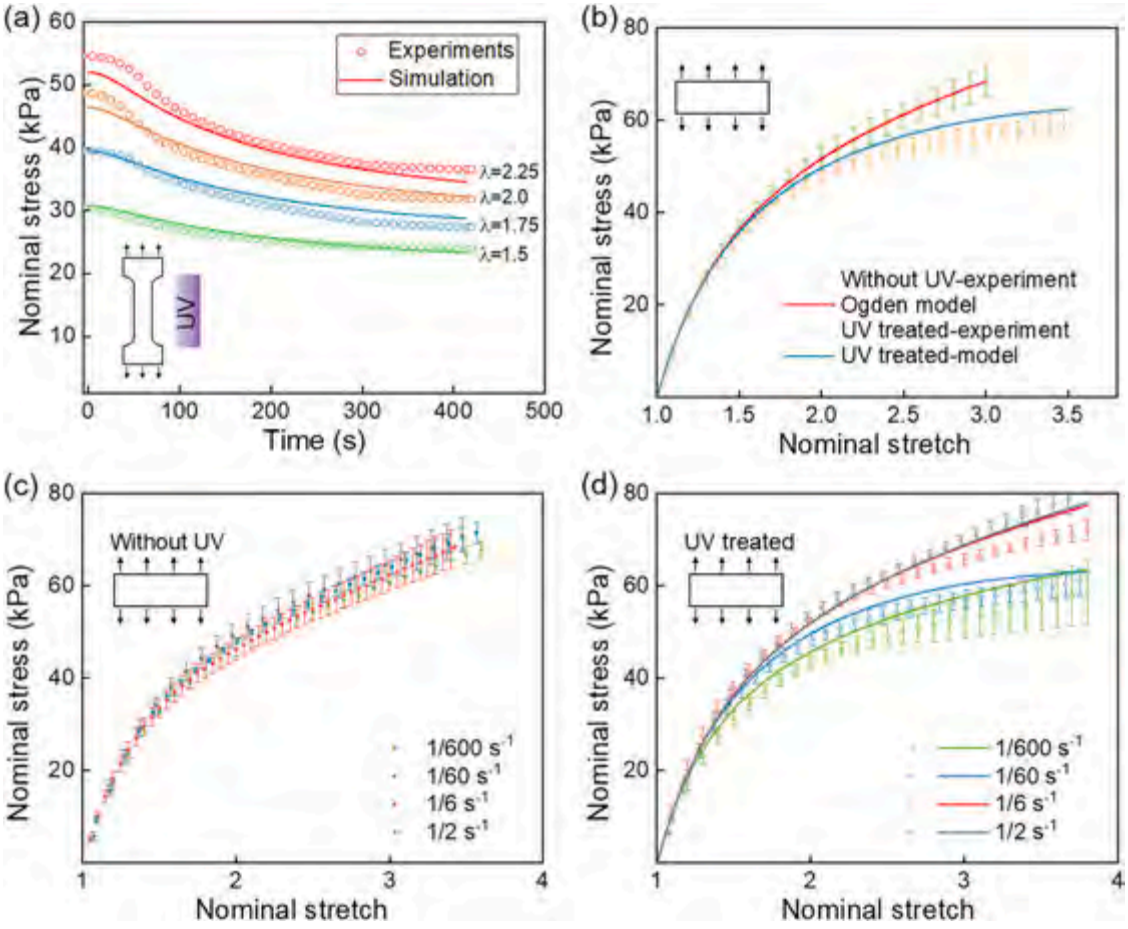

Fig. 6. Experiments and simulation for (a) uniaxial relaxation of the dynamic hydrogel under different fixed stretches, and (b) nominal stress-stretch curves for pure-shear specimens obtained at a stretch rate of $1/60\ s^{-1}$. (c) Nominal stress-stretch curves for unnotched pure-shear specimens obtained at various stretch rates without UV. (d) Nominal stress-stretch curves for pure-shear specimens obtained at various stretch rates under UV. Solid curves are predictions based on the constitutive model. The concentration of BAC in the samples is 0.05 wt%, and PI is 0.5 wt%.

$$\boldsymbol{D}_{vp} = \frac{3}{2}\dot{\epsilon}_p \frac{\boldsymbol{T}}{\sigma_{eq}} = \frac{3}{2}\zeta C_R(t)\boldsymbol{T}. \tag{13}$$

Verification of the constitutive model. The flow rule in Eq. (13) was derived based on the results of a series of uniaxial creep experiments that were performed under UV illumination. Here we show the results of a number of mechanical tests performed under different loading and geometrical conditions, along with the predictions obtained using the constitutive model and the values of the model parameters determined earlier. Fig. 6a shows the evolution of the Cauchy stress during a uniaxial relaxation experiment under UV illumination. Experimental results are shown for various levels of applied stretch, along with the predictions of the constitutive model.

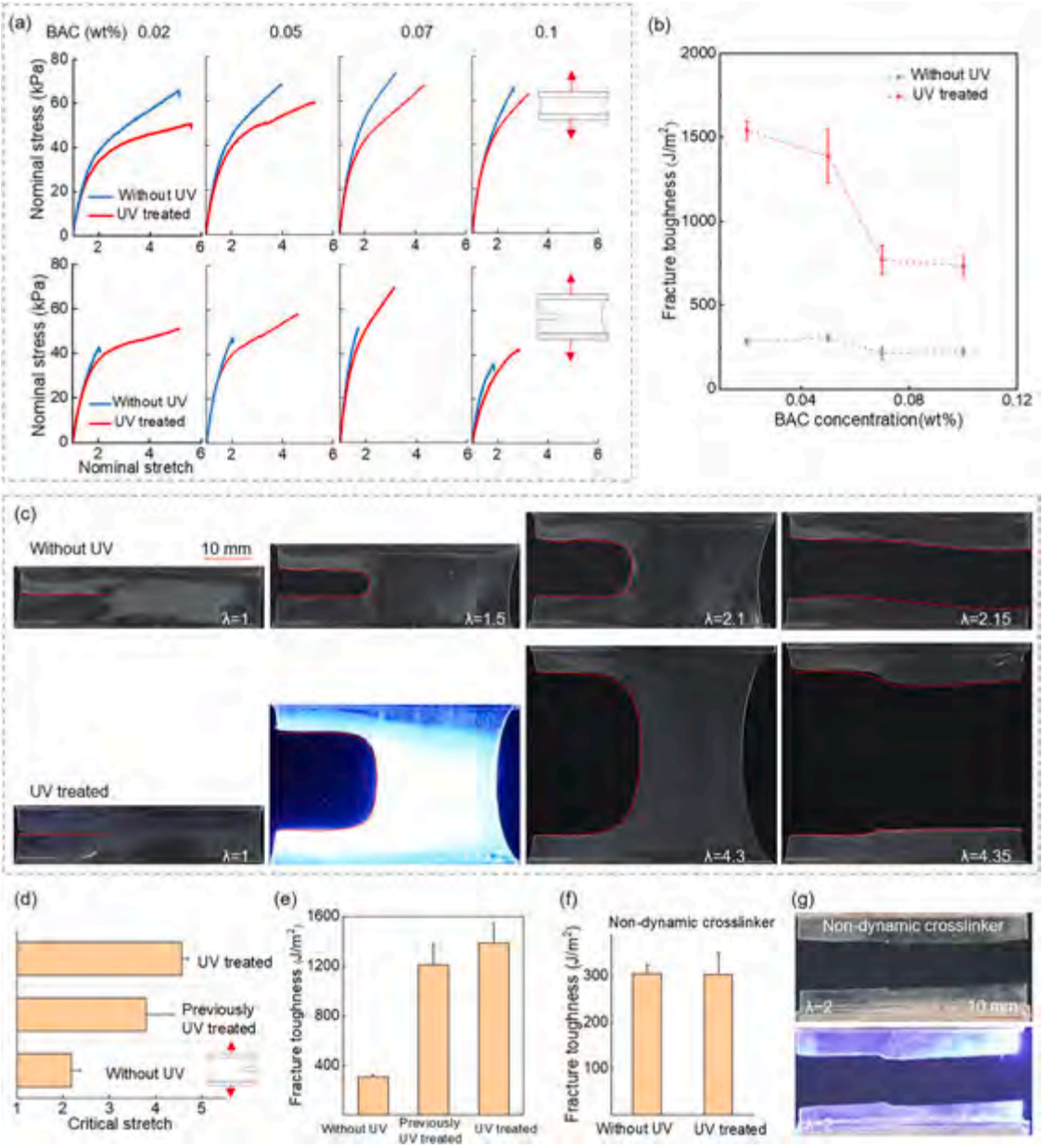

Fig. 7. Fracture of hydrogel with dynamic bonds. (a) Stress-stretch curve of pure-shear specimens with/without UV treatment and with different BAC concentrations. The top row of figures were obtained for specimens without pre-cracks, and the bottom row for specimens with pre-cracks. (b) Fracture toughness of samples with different BAC concentrations. (c) Optical images for pre-cracked hydrogel specimens stretched with/without UV. (d) Critical stretches for specimens with pre-cracks; specimens were tested without UV treatment, after UV treatment for three minutes, and during UV treatment. (e) Corresponding fracture toughness of hydrogel specimens. (f) Fracture toughness of hydrogels crosslinked by a non-dynamic crosslinker (N,N-Methylenebisacrylamide, MBAA) for reference. (g) Optical images for hydrogels with non-dynamic crosslinker. The BAC concentration of the samples is 0.05 wt%.

It is evident that both the magnitude of the stress and its variation with time are in good agreement with the model. Fig. 6b shows the stress-stretch curves for pure-shear experiments both without and with UV illumination. Fig. 6c and d show stress-stretch curves for pure-shear experiments obtained without and with UV illumination, respectively, for various stretch rates. The model curves were obtained by integrating the constitutive model for the pure-shear geometry and are again in good agreement with the experimental results. The pure-shear results, both experimental and model predictions, will be used later to evaluate the fracture properties of the hydrogel.

3.3. Fracture toughness

As shown above, the dynamic reaction relaxes the stress in a hydrogel that has been stretched. Based on this observation, we hypothesize that the viscoplasticity induced by the dynamic process also changes how the hydrogel fractures. Using an approach well established in the literature (Bai et al., 2019; Creton and Ciccotti, 2016; Long et al., 2021; Tang et al., 2017; Zhang et al., 2018a, 2018b), we measure the toughness of the hydrogel by performing pure-shear test on both specimens with and without pre-cracks. The toughness $\boldsymbol{\Gamma}$ is then determined as follows (Bai et al., 2019; Creton and Ciccotti, 2016; Tang et al., 2017; Zhang et al., 2018a, 2018b),

$$\Gamma = HW(\lambda_c), \tag{13}$$

where H is the initial height of the specimen, $W(\lambda)$ is the energy density of a pure-shear specimen without pre-crack and deformed to a stretch λ, and λ_c is the critical stretch at which a specimen with pre-crack fails. The energy density W has the form

$$W(\lambda) = \int_1^{\lambda} S d\lambda, \tag{14}$$

where S is the nominal stress. We performed measurements both with and without UV illumination. For specimens without pre-cracks, the stretch at fracture is greater under UV illumination, but the difference is relatively small. Specimens with pre-cracks, on the other hand, fracture at much greater values of stretch with the UV treatment, and this effect occurs over a broad range of BAC concentrations (Fig. 7a). Evidently, the fracture toughness of hydrogels with UV treatment is approximately three to six times larger than that of hydrogels without treatment (Fig. 7b), depending on the BAC concentration. The energy dissipation associated with the viscoplastic flow at the crack tip has a significant effect on the toughness of the hydrogel. The quantity Γ/W_c, where W_c represents the work of fracture, i.e., the area under the stress-stretch curve, is a length scale that determines how a material is affected by the presence of a flaw. If a flaw in a sample is smaller than this length scale, the fracture strain of the sample is insensitive to the flaw. If the flaw is larger, however, the fracture strain of the sample is reduced by the flaw. It is clear from the results in Fig. 7a and b that UV illumination results in a significant increase in this length scale and that the hydrogel is less flaw sensitive under UV illumination. This effect is especially strong at small BAC concentrations when the crosslink density is relatively low. The difference in fracture behavior is illustrated using optical images in Figs. 7c, S3, and Supplementary Video 1.

UV treatment for three minutes immediately prior to the fracture test also results in an enhanced critical stretch and fracture toughness, as a result of viscoplastic flow in the hydrogel (Fig. 7d, e), although the increase is not as large as for samples that are treated during the measurement. This result suggests that UV illumination has an effect that outlasts the actual UV treatment. We show later that the same is true to an even larger extent for the fatigue behavior of the gels. As a reference, we have also measured the fracture

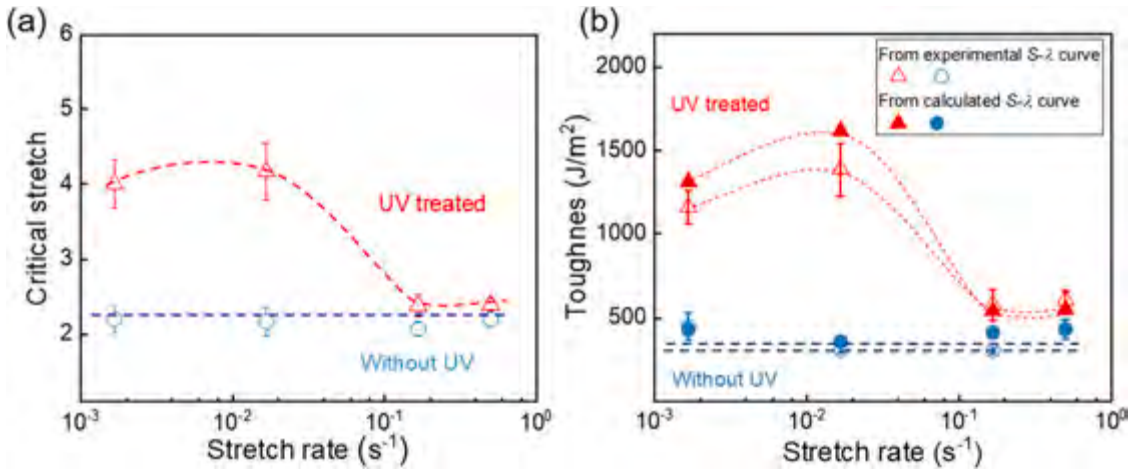

Fig. 8. Fracture toughness of the dynamic hydrogel at different stretch rates. (a) The critical stretches for pre-cracked pure-shear specimens under different stretch rates. (b) Experimental toughness values derived using experimental and calculated stress-strain curves for various stretch rates. The concentration of BAC in the samples is 0.05 wt%, and PI is 0.5 wt%.

toughness of hydrogels crosslinked by a non-dynamic crosslinker. The fracture toughness of these gels is obviously independent of whether the measurements are conducted with or without UV treatment (Fig. 7f, g, Supplementary Video 2).

The viscoplastic flow depends on the concentration of the radicals that are generated in the gel as a result of UV irradiation. Since this concentration varies with time, the mechanical behavior of the hydrogel should depend on the deformation rate. This is not an intrinsic rate dependence. Instead, we consider it an extrinsic dependence where the concentration of radicals available for viscoplastic flow changes depending on the duration of the UV treatment and the time it takes to deform the material. In addition to the effect of the radical concentration, there is also an intrinsic rate effect where, for a fixed concentration of radicals, the stress scales linearly with the viscoplastic strain rate (Eq. (8)). The rate effect is illustrated in Figs. 6 and 8. Fig. 6c and d show experimental stretch-stress curves for unnotched pure-shear specimens obtained at different stretch rates, both without and with UV treatment. The critical stretches for specimens with pre-cracks are shown in Fig. 8a. Without UV treatment, the critical stretches are relatively small and independent of the stretch rate. With UV treatment, the situation is different: for low stretch rates, there is sufficient time for the radicals to react with crosslinks, thus lowering the stress in the hydrogel, dissipating energy, and increasing the resistance to fracture. When the stretch speed is high ($>0.1\ s^{-1}$), by contrast, the hydrogel fails quickly, because there are insufficient radicals and insufficient time to affect the network in a meaningful way. As a result, the critical stretch is nearly the same as for materials without UV treatment. Fig. 6d shows model predictions of the nominal stress-stretch curves of UV-treated specimens for several strain rates. When these curves are combined with the experimental values of the critical stretches shown in Fig. 8a, the toughness of the gel can be calculated as a function of stretch rate. These results are summarized in Fig. 8b, alongside the toughness values evaluated using the experimental stress-stretch curves. There is clearly good agreement between both calculation methods. Furthermore, the figure demonstrates the rather significant effect of the UV treatment on the toughness of the hydrogel, provided the stretch rate is sufficiently small to allow for meaningful viscoplastic flow.

In summary, there are two scenarios depending on the deformation rate: (1). If the stretch rate is low, the radical concentration peaks when there is significant network deformation, the crosslinks reconfigure, and the hydrogel has a high toughness; (2). If the stretch rate is too high, the hydrogel fails before the radicals have a significant effect on the network.

Using the photochemical model, it is possible to estimate the timescale required to generate radicals upon UV illumination. The concentration of radicals reaches a maximum after an illumination time t_p given approximately by

$$t_p \approx \frac{2}{\beta I}\ln\left(\frac{0.9+\gamma}{0.982\gamma}\right) \text{ with } \gamma = \sqrt{\frac{C_o k_o m}{\beta I}}, \tag{15}$$

where C_o is the initial concentration of photoinitiator. This expression allows us to define a non-dimensional stretch rate $\dot{\Lambda}$.

$$\dot{\Lambda} = \frac{\dot{\lambda} t_p}{\lambda_c - 1} = \frac{2\dot{\lambda}_t}{(\lambda_c - 1)\beta I}\ln\left(\frac{0.9+\gamma}{0.982\gamma}\right) \tag{16}$$

where $\dot{\lambda}$ is the nominal stretch rate. The stretch rate $\dot{\lambda}$ for which the non-dimensional stretch rate $\dot{\Lambda}$ is on the order of one should result in the greatest possible effect of UV illumination on the hydrogel toughness. Given the various fitting parameters obtained for the photochemical model and the values of the critical stretch in Fig. 8, we find that $\dot{\lambda} \approx 2.2 \times 10^{-2}\ s^{-1}$, in good agreement with the experimental results shown in the same figure.

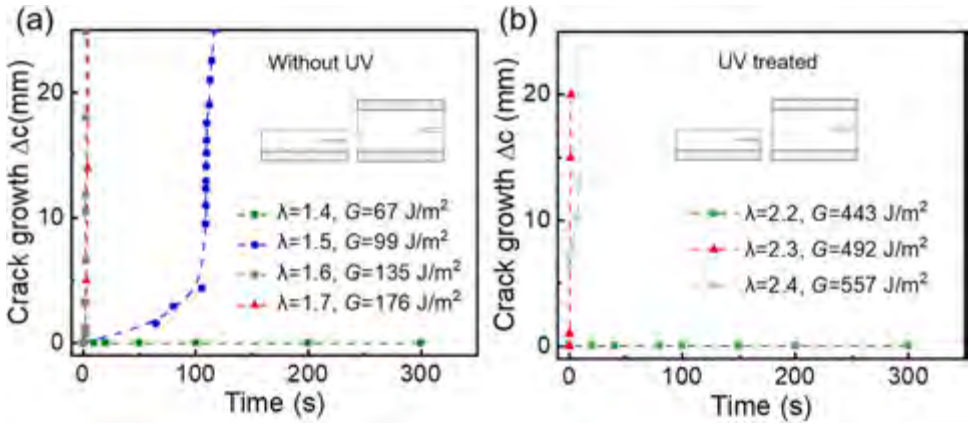

Fig. 9. Delayed fracture. (a) Crack growth curves for hydrogel specimens without UV treatment and (b) with UV treatment for various levels of applied stretch λ. The concentration of BAC is 0.1 wt% and PI is 0.5 wt%. The values of the energy release rate G listed in the figures are obtained from the stress-stretch curves of pure-shear specimens without consideration of stress relaxation.

3.4. Delayed fracture

Single-network hydrogels are susceptible to delayed fracture (Bai et al., 2019; Tang et al., 2017). Instead of growing instantaneously, under some conditions, a crack in a hydrogel may grow very slowly at first and then suddenly grow very rapidly. Delayed fracture has been attributed to viscoelastic or poroelastic effects, as well as to subcritical crack growth as a result of chemically assisted chain scission at the crack tip, (Bonn et al., 1998; Lindström et al., 2012; Wang and Hong, 2012). Here we evaluate the effect of UV treatment on delayed fracture. Samples with pre-cracks are deformed to a predefined stretch and then the crack length is monitored as a function of time using a camera. For samples without UV treatment, delayed fracture occurs when the applied stretch reaches a value of 1.5 (Figs. 9a, S4), well below the critical stretch. The precise mechanism responsible for delayed fracture in this hydrogel is not known at this time. One possible mechanism may be stress-assisted hydrolysis of the amide moiety in the crosslinker, but this would need to be confirmed experimentally, for instance by evaluating the effect of pH on crack velocity. While visco-elastic effects are likely not responsible for delayed fracture in this hydrogel, poroelastic effects cannot be ruled out (Karobi et al., 2016; Wang and Hong, 2012; Yu et al., 2018).

Samples that are UV-treated do not show any crack growth until a stretch greater than 2.2 is applied, at which point cracks grow rapidly (Fig. 9b). This applied stretch corresponds to the critical fracture stretch for the deformation rate used in the experiments. We believe that the lack of crack growth for smaller stretches arises because UV irradiation affects both the applied driving force for crack growth and the resistance to crack growth: When a hydrogel sample under UV illumination is deformed to a predefined stretch, the overall stress in the sample relaxes over time as a result of viscoplastic flow (Fig. 6a), in effect reducing the applied energy release rate. If a crack in the sample does not propagate upon applying a stretch, the sample is less likely to show delayed fracture because the applied energy release rate decreases over time. UV illumination also results in a reduction of the stresses at the crack tip as a result of viscoplastic flow. The associated energy dissipation increases the resistance of the hydrogel to crack growth. If stress-assisted hydrolysis is indeed the relevant crack growth mechanism for delayed fracture, the reduced stress at the crack tip would also make this process more difficult.

3.5. Fatigue fracture

We also evaluated the response of the hydrogel to cyclical loading. This is of interest because crack growth under fatigue conditions can shed light on how cracks propagate through the polymer network of the hydrogel. Although many strategies can be used to enhance the toughness of a hydrogel, these strategies do little to increase the fatigue threshold (Bai et al., 2019; Zhang et al., 2018a). This phenomenon can be understood in the context of the Lake-Thomas model for the fracture of polymers (Creton, 2017; Creton and Ciccotti, 2016; Lake and Thomas, 1967). Assuming that the fatigue threshold arises from the energy required to sever polymer chains

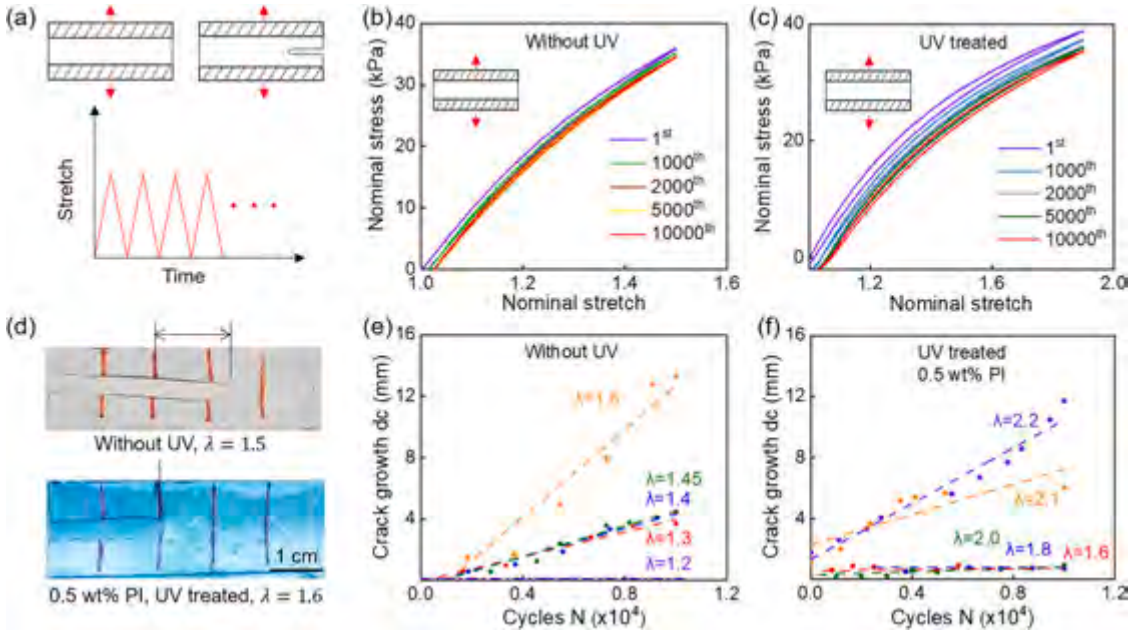

Fig. 10. Fatigue of the dynamic hydrogel. (a) Fatigue test specimen diagram. Specimens without pre-cracks are used to record the stress-stretch curves under cyclical loading; pre-cracked specimens are used to record the crack growth. (b) Examples of stress-stretch curves for unnotched specimens without UV treatment stretched ($\lambda_{max} = 1.5$) (c) and with UV treatment ($\lambda_{max} = 1.9$. (d) Photographs of pre-cracked specimens and crack growth after 10,000 cycles. (e, f) Crack growth for notched specimens without/with UV treatment, for various applied stretches. The concentration of BAC in the samples is 0.05 wt%, and PI is 0.5 wt%.

in the immediate vicinity of the crack tip only (Creton, 2017; Creton and Ciccotti, 2016; Lake and Thomas, 1967; Tang et al., 2017) and that the small amplitude of the cyclic load at the fatigue threshold is insufficient to activate bulk energy dissipation mechanisms, the fatigue threshold of a hydrogel can be estimated as (Bai et al., 2019; Tang et al., 2017; Zhang et al., 2018a, 2018b; Zhou et al., 2020)

$$\Gamma_0 = \phi^{2/3}\sqrt{M}blU, \tag{17}$$

where M is the average number of monomers in a polymer chain between two crosslinks, b is the number of C-C bonds per unit volume, l is the length of the monomer unit, ϕ is the volume fraction of the polymer in the hydrogel, and U is the single C-C bond energy. For instance, monomer and crosslinker concentrations of 4 mol/L and 1.92×10^{-3} mol/L, respectively, yields a value of $M = 1042$ (Bai et al., 2019; Creton and Ciccotti, 2016; Zhou et al., 2020). We take $\phi = 26\%$ based on the recipe used for hydrogel synthesis. Using previously reported values for $b = 1.22 \times 10^{28}$ m^{-3}, $l = b^{-1/3} = 0.43$ nm, and $U = 3.3 \times 10^{-19}$ J (Lake and Thomas, 1967; Tang et al., 2017), we obtain a fatigue threshold $\Gamma_0 = 23$ J/m^2.

We performed extensive fatigue experiments on the hydrogels, both with and without pre-cracks (Fig. 10a). First, specimens without pre-cracks were tested to determine the energy release rates from their stress-stretch curves. The stress-stretch curves of specimens that were tested in the absence of UV were very nearly elastic over 10,000 cycles (Fig. 10b). The stress-stretch curves of specimens that were tested under UV illumination, by contrast, showed more pronounced hysteresis, especially in the early stage of the experiment when the radical concentration is high (Fig. 10c).

Pre-cracked samples tested in the absence of UV showed crack growth at low energy release rates, but samples tested under UV illumination at the same or slightly higher energy release rates did not (Fig. 10d). The crack growth results are summarized in Fig. 10e and f. Samples with pre-cracks that were tested without UV illumination show significant crack growth even at stretches as small as $\lambda = 1.3$ (Fig. 10e); samples tested under UV illumination show crack growth only when the stretch exceeds $\lambda = 2.0$ (Fig. 10f). Evidently, viscoplastic flow at the crack tip early on in the fatigue experiment when the radical concentration is high, reduces the stress state at the crack tip later on in the experiment. Furthermore, viscoplastic flow also reduces the overall stress state in the sample and hence the applied energy release rate (Fig. 10c).

Fig. 11 shows crack growth rates as a function of the energy release rate for various test conditions. Extrapolating the crack growth rates to zero provides rough estimates of the fatigue thresholds. The threshold for hydrogels tested without UV illumination is only ~19 J/m^2, while the threshold for the tests with the two different UV treatments is in the range of 40–200 J/m^2. The value of the fatigue threshold in the absence of UV is in good agreement with the estimate from the Lake-Thomas model. Evidently, the amplitude of the cyclic load at the threshold is insufficient to activate bulk energy dissipation mechanisms in the material. If, however, the material is exposed to UV, the fatigue threshold increases significantly. This increase in the threshold upon UV exposure is much larger than can be explained by a change in the value of M in the Lake-Thomas model, which must be very small considering the minimal change in material stiffness on UV exposure. This observation suggests that the increase in the fatigue threshold of the material is the result of UV radiation-mediated viscoplastic flow at the crack tip and the concomitant reduction in the stress concentration at the crack tip. As such, we expect the fatigue threshold to be deformation-rate dependent, both because of the variable concentration of the radicals in the hydrogel and the intrinsic rate dependence of the flow rule.

4. Summary

In this study, we investigated the deformation and fracture behavior of a hydrogel with UV-controllable dynamic crosslinks. The mechanical behavior of the hydrogel under various conditions including uniaxial stretching, creep, and relaxation, are well described by a model that allows for viscoplastic flow through a continuous process of severing and reforming crosslinks as a result of radicals

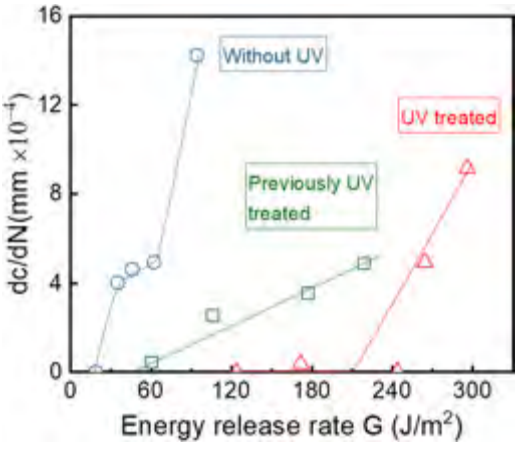

Fig. 11. Crack growth rates as a function of applied energy release rate for samples without and with UV treatment. The concentration of BAC is 0.05 wt%, and PI 0.5 wt%.

generated by UV irradiation. Experiments show that the viscoplastic flow has a linear dependence on stress and that the evolution of the free radicals in the hydrogel is well described by a photochemical model. Our results further show that this dynamic process of severing and reforming crosslinks has a significant impact on the fracture behavior of the hydrogel. UV irradiation results in a significant increase of the fracture toughness, the threshold for delayed fracture, and the fatigue threshold of the hydrogel.

CRediT authorship contribution statement

Hang Yang: Visualization, Methodology, Supervision, Formal analysis, Writing – original draft. **Xi Chen:** Supervision, Formal analysis, Methodology. **Bonan Sun:** Methodology. **Jingda Tang:** Supervision, Formal analysis. **Joost J. Vlassak:** Visualization, Supervision, Formal analysis, Writing – original draft.

Declaration of Competing Interest

The authors declare no competing interest.

Data Availability

Data will be made available on request.

Acknowledgments

This research was supported by the Harvard University MRSEC, which is funded by the National Science Foundation under Grant DMR-2011754. Part of this work was performed at the Center for Nanoscale Systems (CNS), which is supported by the National Science Foundation under Grant ECS 1541959. JT acknowledges support from the National Natural Science Foundation of China (No. 12172272).

Supplementary materials

Supplementary material associated with this article can be found, in the online version, at doi:10.1016/j.jmps.2022.105083.

References

An, L., Shi, Q., Jin, C., Zhao, W., Wang, T., 2022. Chain diffusion based framework for modeling the welding of vitrimers. J. Mech. Phys. Solids 164, 104883.
Bai, R., Yang, J., Suo, Z., 2019. Fatigue of hydrogels. Eur. J. Mech. A Solids 74, 337–370.
Bonn, D., Kellay, H., Prochnow, M., Ben-Djemiaa, K., Meunier, J., 1998. Delayed fracture of an inhomogeneous soft solid. Science 280, 265–267.
Chen, D., Zhang, Y., Ni, C., Ma, C., Yin, J., Bai, H., Luo, Y., Huang, F., Xie, T., Zhao, Q., 2019. Drilling by light: ice-templated photo-patterning enabled by a dynamically crosslinked hydrogel. Mater. Horiz. 6, 1013–1019.
Creton, C., 2017. 50th anniversary perspective: networks and gels: soft but dynamic and tough. Macromolecules 50, 8297–8316.
Creton, C., Ciccotti, M., 2016. Fracture and adhesion of soft materials: a review. Reports on progress in physics. Phys. Soc. 79, 046601.
Du, X., Li, J., Welle, A., Li, L., Feng, W., Levkin, P.A., 2015. Reversible and rewritable surface functionalization and patterning via photodynamic disulfide exchange. Adv. Mater. 27, 4997–5001.
Fairbanks, B.D., Schwartz, M.P., Bowman, C.N., Anseth, K.S., 2009. Photoinitiated polymerization of PEG-diacrylate with lithium phenyl-2, 4, 6-trimethylbenzoylphosphinate: polymerization rate and cytocompatibility. Biomaterials 30, 6702–6707.
Fairbanks, B.D., Singh, S.P., Bowman, C.N., Anseth, K.S., 2011. Photodegradable, photoadaptable hydrogels via radical-mediated disulfide fragmentation reaction. Macromolecules 44, 2444–2450.
Gong, J.P., Katsuyama, Y., Kurokawa, T., Osada, Y., 2003. Double-network hydrogels with extremely high mechanical strength. Adv. Mater. 15, 1155–1158.
Guo, J., Liu, M., Zehnder, A.T., Zhao, J., Narita, T., Creton, C., Hui, C.Y., 2018. Fracture mechanics of a self-healing hydrogel with covalent and physical crosslinks: a numerical study. J. Mech. Phys. Solids 120, 79–95.
Guo, J., Long, R., Mayumi, K., Hui, C.Y., 2016. Mechanics of a dual cross-link gel with dynamic bonds: steady state kinetics and large deformation effects. Macromolecules 49, 3497–3507.
Jiang, H., Zhang, G., Li, F., Zhang, Y., Lei, Y., Xia, Y., Jin, X., Feng, X., Li, H., 2017. A self-healable and tough nanocomposite hydrogel crosslinked by novel ultrasmall aluminum hydroxide nanoparticles. Nanoscale 9, 15470–15476.
Karobi, S.N., Sun, T.L., Kurokawa, T., Luo, F., Nakajima, T., Nonoyama, T., Gong, J.P., 2016. Creep behavior and delayed fracture of tough polyampholyte hydrogels by tensile test. Macromolecules 49, 5630–5636.
Kim, J., Zhang, G., Shi, M., Suo, Z., 2021. Fracture, fatigue, and friction of polymers in which entanglements greatly outnumber cross-links. Science 374, 212–216.
Lake, G., Thomas, A., 1967. The strength of highly elastic materials. Proc. R. Soc. Lond. Ser. A Math. Phys. Sci. 300, 108–119.
Li, J., Mooney, D.J., 2016. Designing hydrogels for controlled drug delivery. Nat. Rev. Mater. 1 (12), 1–17.
Li, X., Cui, K., Kurokawa, T., Ye, Y.N., Sun, T.L., Yu, C., Creton, C., Gong, J.P., 2021. Effect of mesoscale phase contrast on fatigue-delaying behavior of self-healing hydrogels. Sci. Adv. 7, eabe8210.
Li, X., Gong, J.P., 2022. Role of dynamic bonds on fatigue threshold of tough hydrogels. Proc. Natl. Acad. Sci. 119, e2200678119.
Lin, P., Ma, S., Wang, X., Zhou, F., 2015. Molecularly engineered dual-crosslinked hydrogel with ultrahigh mechanical strength, toughness, and good self-recovery. Adv. Mater. 27, 2054–2059.
Lin, S., Liu, J., Liu, X., Zhao, X., 2019a. Muscle-like fatigue-resistant hydrogels by mechanical training. Proc. Natl. Acad. Sci. 116, 10244–10249.
Lin, S., Liu, X., Liu, J., Yuk, H., Loh, H.C., Parada, G.A., Settens, C., Song, J., Masic, A., McKinley, G.H., 2019b. Anti-fatigue-fracture hydrogels. Sci. Adv. 5, eaau8528.
Lindström, S.B., Kodger, T.E., Sprakel, J., Weitz, D.A., 2012. Structures, stresses, and fluctuations in the delayed failure of colloidal gels. Soft Matter 8, 3657–3664.

Liu, X., Liu, J., Lin, S., Zhao, X., 2020. Hydrogel machines. Mater. Today 36, 102–124.
Long, K.N., Scott, T.F., Jerry Qi, H., Bowman, C.N., Dunn, M.L., 2009. Photomechanics of light-activated polymers. J. Mech. Phys. Solids 57, 1103–1121.
Long, R., Hui, C.Y., Gong, J.P., Bouchbinder, E., 2021. The fracture of highly deformable soft materials: a tale of two length scales. Annu. Rev. Condens. Matter Phys. 12, 71–94.
Long, R., Mayumi, K., Creton, C., Narita, T., Hui, C.Y., 2014. Time dependent behavior of a dual cross-link self-healing gel: theory and experiments. Macromolecules 47, 7243–7250.
Ma, J., Mu, X., Bowman, C.N., Sun, Y., Dunn, M.L., Qi, H.J., Fang, D., 2014. A photoviscoplastic model for photoactivated covalent adaptive networks. J. Mech. Phys. Solids 70, 84–103.
Ogden, R.W., 1972. Large deformation isotropic elasticity–on the correlation of theory and experiment for incompressible rubberlike solids. Proc. R. Soc. Lond. A Math. Phys. Sci. 326, 565–584.
Sun, J.Y., Zhao, X., Illeperuma, W.R., Chaudhuri, O., Oh, K.H., Mooney, D.J., Vlassak, J.J., Suo, Z., 2012. Highly stretchable and tough hydrogels. Nature 489, 133–136.
Sun, T.L., Kurokawa, T., Kuroda, S., Ihsan, A.B., Akasaki, T., Sato, K., Haque, M.A., Nakajima, T., Gong, J.P., 2013. Physical hydrogels composed of polyampholytes demonstrate high toughness and viscoelasticity. Nat. Mater. 12, 932–937.
Tang, J., Li, J., Vlassak, J.J., Suo, Z., 2017. Fatigue fracture of hydrogels. Extreme Mech. Lett. 10, 24–31.
Venkata, S.P., Cui, K., Guo, J., Zehnder, A.T., Gong, J.P., Hui, C.Y., 2021. Constitutive modeling of bond breaking and healing kinetics of physical Polyampholyte (PA) gel. Extreme Mech. Lett. 43, 101184.
Wang, X., Hong, W., 2012. Delayed fracture in gels. Soft Matter 8, 8171–8178.
Wang, Z., Xiang, C., Yao, X., Le Floch, P., Mendez, J., Suo, Z., 2019. Stretchable materials of high toughness and low hysteresis. Proc. Natl. Acad. Sci. U. S. A. 116, 5967–5972.
Wang, Z., Zheng, X.J., Ouchi, T., Kouznetsova, T., Beech, H., Av-Ron, S., Bowser, B., Wang, S., Johnson, J., Kalow, J., 2021. Toughening hydrogels through force-triggered chemical reactions that lengthen polymer. strands.Science 374 (6564), 193–196.
Weber, G., Anand, L., 1990. Finite deformation constitutive equations and a time integration procedure for isotropic, hyperelastic-viscoplastic solids. Comput. Methods Appl. Mech. Eng. 79, 173–202.
Xiang, C., Wang, Z., Yang, C., Yao, X., Wang, Y., Suo, Z., 2020. Stretchable and fatigue-resistant materials. Mater. Today 34, 7–16.
Xiao, Y., Li, Q., Yao, X., Bai, R., Hong, W., Yang, C., 2022. Fatigue of amorphous hydrogels with dynamic covalent bonds. Extreme Mech. Lett. 53, 101679.
Yang, C., Suo, Z., 2018. Hydrogel ionotronics. Nat. Rev. Mater. 3, 125–142.
Yang, H., Ji, M., Yang, M., Shi, M., Pan, Y., Zhou, Y., Qi, H.J., Suo, Z., Tang, J., 2021. Fabricating hydrogels to mimic biological tissues of complex shapes and high fatigue resistance. Matter 4, 1935–1946.
Yang, J., Bai, R., Chen, B., Suo, Z., 2020. Hydrogel adhesion: a supramolecular synergy of chemistry, topology, and mechanics. Adv. Funct. Mater. 30, 1901693.
Yu, Y., Landis, C.M., Huang, R., 2018. Steady-state crack growth in polymer gels: a linear poroelastic analysis. J. Mech. Phys. Solids 118, 15–39.
Yuk, H., Lu, B., Zhao, X., 2019. Hydrogel bioelectronics. Che. Soc. Rev. 48, 1642–1667.
Zhang, W., Hu, J., Tang, J., Wang, Z., Wang, J., Lu, T., Suo, Z., 2018a. Fracture toughness and fatigue threshold of tough hydrogels. ACS Macro Lett. 8, 17–23.
Zhang, W., Liu, X., Wang, J., Tang, J., Hu, J., Lu, T., Suo, Z., 2018b. Fatigue of double-network hydrogels. Eng. Fract. Mech. 187, 74–93.
Zhang, Y.S., Khademhosseini, A., 2017. Advances in engineering hydrogels. Science 356 (6337), eaaf3627.
Zhao, X., Chen, X., Yuk, H., Lin, S., Liu, X., Parada, G., 2021. Soft materials by design: unconventional polymer networks give extreme properties. Chem. Rev. 121, 4309–4372.
Zheng, N., Xu, Y., Zhao, Q., Xie, T., 2021. Dynamic covalent polymer networks: a molecular platform for designing functions beyond chemical recycling and self-healing. Chem. Rev. 121, 1716–1745.
Zhou, Y., Zhang, W., Hu, J., Tang, J., Jin, C., Suo, Z., Lu, T., 2020. The stiffness-threshold conflict in polymer networks and a resolution. J. Appl. Mech. 87, 031002.